Supplementary data

Molecular imprinting of complex matrices at localized surface plasmon resonance biosensors for screening of global interactions of polyphenols and proteins

*Joana Rafaela Lara Guerreiro, Vladimir E. Bochenkov, Kasper Runager, Hüsnü Aslan, Mingdong Dong, Jan J. Enghild, Victor De Freitas, Maria Goreti Ferreira Sales and Duncan S. Sutherland**

ABSTRACT:

Detailed materials and methods are described in this section. The supplementary data includes the synthesis procedure of two small molecules (the polyphenol PGG and procyanidin dimer B3), the protein characterization of saliva and amylase, the Au nanodisks fabrication based on colloidal lithography, the edification and evaluation of molecular imprinted polymer around the nanostructures, the interaction measurements between saliva or amylase and the three polyphenols followed by the LSPR sensor. Additional control measurements were also performed by electrochemistry in Au bare electrodes. Molecular imprinted and non-imprinted layers on Au nanodisks were also characterized by Atomic Force Microscopy (AFM). Identification of the salivary proteins recognized by the saliva imprinted material was conducted by mass spectroscopy of both pure saliva and Au disks/MIP saliva/rebinding.

Table of contents

1. Materials and Methods

Glass coverslips (#3, 25 mm diameter) were purchased from Menzel-gläser and SPR sensor chip Au purchased from GE Healthcare. SPR chips were cleaned in acetone, ethanol, MQ water (MilliQ gradient, Milipore) and UV ozone prior spin coat with PMMA A4 (Polymethylmethacrylate) Mw 495,000, 4% anisole purchased from Micro resist technology GmbH (Germany). PDDA (poly(diallyldimethylammonium chloride)), PSS (poly(sodium-4-styrenesulfonate)) were purchased from Sigma-Aldrich. PAX-XL60 (polyammonium chloride) was purchased from KemiraMiljø and polystyrene colloidal particles were purchased from Invitrogen.

Thiophenecarboxylic acid (TPCA), Methacrylic Acid (MAA), (vinylbenzyl)trimethylammonium chloride 97% (VTMA), Ethylene Glycol Dimethacrylate 98% (EGDMA), Ammonium Persulfate (AP), Methyl Acrylate 99% (MA), Proteinase k from Engyodontium album, Alpha-Amylase from porcine pancreas (AMY), Potassium Hexacyanoferrate II-3-hydrate, Potassium Hexacyanoferrate III, Phosphate buffered saline (PBS), Potassium Hydroxide (KOH), Sulfuric Acid (H_2SO_4), Hydrogen Peroxide (H_2O_2), Potassium Chloride (KCl), , (+)-Catechin hydrate were purchased from Sigma-Aldrich.

Ammonium Bicarbonate (AMBIC), Trypsin proteomics grade were ordered from Sigma-Aldrich.

Alpha amylase standards were prepared in PBS while polyphenol standards (PGG, Catechin and B3) were prepared in PBS with 5% ethanol (PBS-E).

1.1. β-1,2,3,4,6-Penta-O-galloyl-D-glucopyranose (PGG) Synthesis.

The synthesis of PGG was based on Chen and Hagerman method.[1] Briefly, 5.0 g of tannic acid was methanolyzed in 70% methanol in acetate buffer (0.1 M, pH 5.0) at 65°C for 15 h, with immediate pH adjustment to 6.0 with NaOH. Methanol was evaporated under reduced pressure at <30 °C, and water was added to maintain the volume. The solution was extracted with 3 volumes of diethyl ether and 3 volumes of ethyl acetate. The ethyl acetate extracts were combined and evaporated, with addition of water to maintain the volume. The resulting suspension was centrifuged and the precipitate was redissolved by heating in 2% methanol solution. PGG precipitation occurred by cooling it down to room temperature and it was collected by centrifugation. PGG was washed twice with an ice-cold 2% methanol solution and once with ice-cold distilled water. The final product was lyophilized to yield a white powder with an

overall mass yield of 23%. The purity of the obtained PGG was assessed by HPLC analysis and 1H NMR spectroscopy, and it was ≤99%.[2]

1.2. B3 synthesis

The synthesis of procyanidin dimer B3 (catechin-(4-8)-catechin) followed the procedure described by Bras et al.[3] Briefly, both taxifolin and (+)-catechin (ratio 1:3) were dissolved in ethanol and treated with sodium borohydride (in ethanol). Followed by the addiction of CH_3CO_2H/H_2O 50% (v/v) to lower down the pH to 4.5 and kept under argon atmosphere for 30 min. The mixture was extracted with ethyl acetate. After solvent evaporation, water was added and the mixture was passed through C18 gel, washed with water, and recovered with methanol. After methanol evaporation, the fraction was passed through a TSK Toyopearl HW-40(s) gel column (300 mm × 10 mm i.d., 0.8 mL.min-1, methanol as eluent) coupled to a UV-vis detector. Several fractions were recovered and analyzed by ESI-MS (Finnigan DECA XP PLUS) yielding procyanidins dimers (B3). The structure was elucidated by HPLC-MS and NMR analysis.

2. Au nanodisks fabrication

The glass substrates were cleaned in acetone followed by plasma cleaning (RF 100 watts, pressure 25mtorr for 15 minutes). PMMA was spin coated at 3000 rpm and 1000 r/sec^2 for 1 min followed by 2 min in a hot plate. The nanostructured surfaces were made by sparse colloidal lithography.[4] The colloidal mask involved the deposition of a triple layer of polyelectrolytes i) 2% PDDA ii) 2% PSS and iii) 5% PAX-XL60 for 30 min each and by the respective order. The colloidal monolayer of charged polystyrene particles 100 nm sizes (0.2% w/w in MQ) was then deposited on the surface for 120 s followed by rinsing in MQ water and dried under a stream of nitrogen gas. The coating process of the pretreated glass samples started with the deposition of 20 nm Ti (3×10-8 torr argon pressure, Ti deposition rate 1Å/s). The particles were then removed by tape stripping followed by etching for 10 min (RF 50 watts, pressure 25mtorr) which removed the PMMA layer from the exposed spots provided by particles removal. Afterwards, samples were again coated with 2 nm Ti and 20 nm Au (3×10-8 torr argon pressure, Ti deposition rate 1Å/s). Au coated samples were rinsed with acetone until PMMA removal with metal layer on top. Therefore, the nanostructured samples were rinsed with acetone, ethanol and MQ cleaned for 3 min each, in the sonicator. After drying the samples under a stream of nitrogen gas, samples where cleaned for 1 h in UV/ozone followed by 1 h in MQ water to reduce the oxidized Au back to Au(0).

Scanning Electron Microscopy (Magellan™ XHR SEM, FEI) was used to characterized the samples and determine disks size and inter-disks distance. The diameter distribution of each patch size was measured using ImageJ. The Au nanopattern fabricated on a glass substrate showed cylindrical disks (**Figure S-1**), with a diameter of 99±4 nm and distribution of ~18 disks/μm^2.

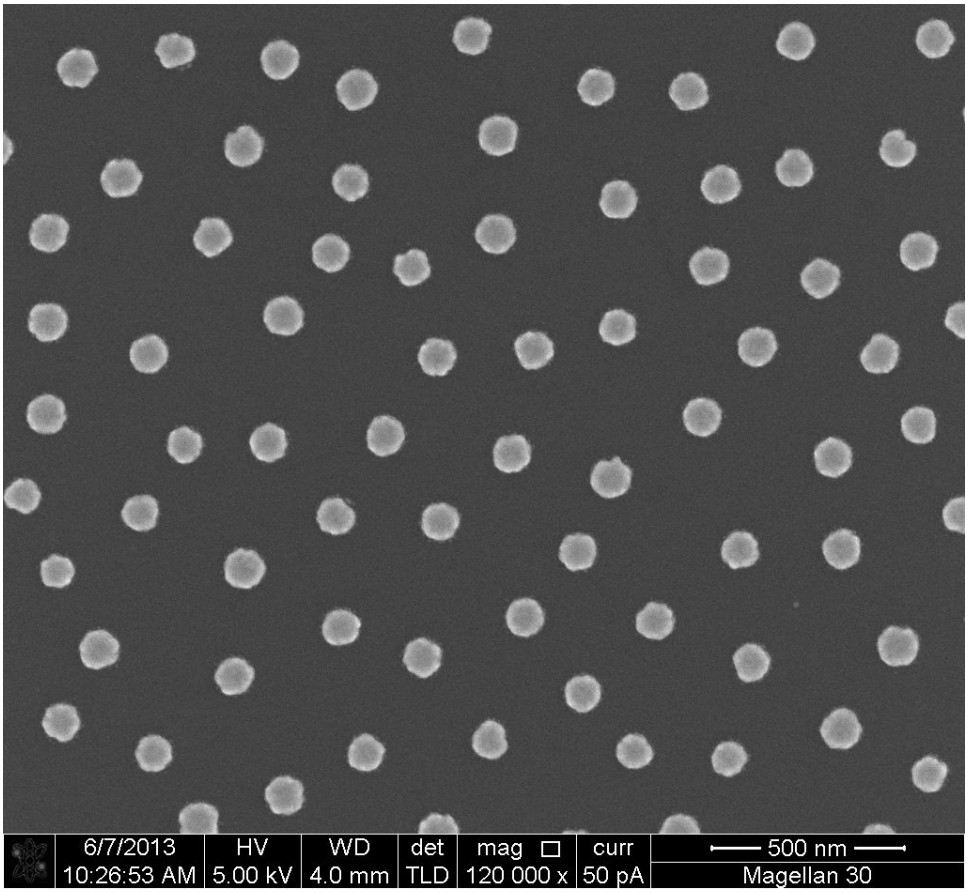

Figure S -1 – SEM image of Au nanodisks pattern.

3. Saliva

3.1. Saliva Collection

Whole-mouth saliva was collected from healthy volunteers with ages ranging from 23–30. And it was made by expectorating saliva into a small falcon tube periodically over about 15 min. Volunteer's reported not having consumed any food or drink other than water for at least 1 h before saliva collection. The collected volume ~6 mL of saliva from each volunteer was used to make a saliva pool (whole saliva). Saliva from all volunteers was centrifuge for 5 minutes at 1300 g at 4 °C to remove undissolved

materials. Aliquots of 2 ml of resulting supernatants were then stored at -20 °C. Saliva was allowed to equilibrate to room temperature (~20°C) before analysis.

4. Protein Characterization

The present work studies the interaction of polyphenol with salivary proteins and in parallel it was also evaluated a specific salivary protein, alpha-amylase. Several compounds can be found in saliva and in terms of proteins compositions it may present a huge variety. Therefore, saliva characterization was required.

4.1. Sodium dodecyl sulfate polyacrylamide gel electrophoresis (SDS-PAGE) of Saliva and Amylase

The samples were prepared by mixing 10 µL of saliva or AMY with 10 µl of sample buffer (Thermo Scientific) and 25 µl of PBS followed by 5 minutes boiling facilitating SDS binding. After cooling down the samples they were loaded onto a 10 well Pierce® 4-20% polyacrylamide precast gel (Thermo Scientific). The gel preparation involved the loading of 5µL of molecular weight standards (Thermo Scientific PageRuler Unstained Protein Ladder) on the first and last lane, whereas pure and diluted saliva was loaded on the 2 to 5 lanes and different AMY concentrations from the 6 to 9 lane of each gel. The staining process used the imperial protein stain from Thermo Scientific, and gel scanning was carried out by Gel DocTM EZ Image r (Bio-Rad) with a white light sample tray (Bio-Rad). Image processing used Image LabTM 4.0.1 Software (Bio-Rad).

Both saliva and AMY with different concentrations were analyzed using SDS-PAGE, **Figure S-2** shows their protein composition

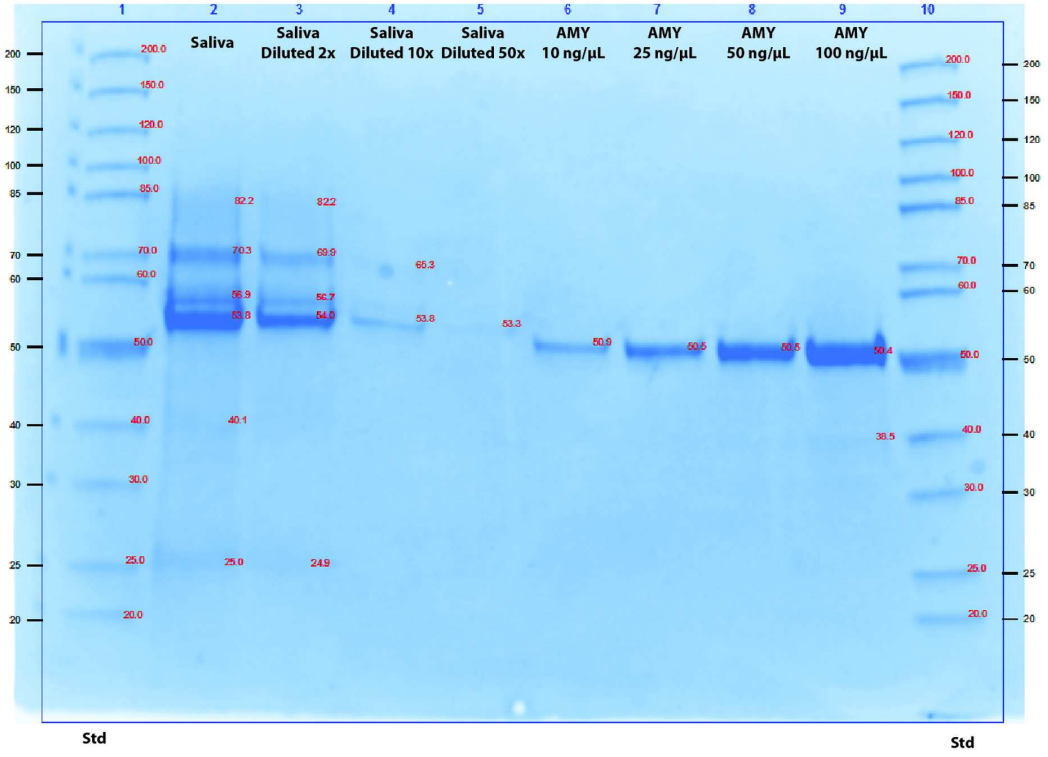

Figure S-2–Gel scan of saliva and AMY proteins, the top part of the gel describes the sample loaded.

Saliva and AMY samples were loaded on the lane 2 to 9 while lane 1 and 10 represents the molecular weight markers. Pure saliva when compared with diluted saliva samples presents the same profile, however dilution increment decreases the bands intensities. The saliva sample displays a faintly band at 82.2 kDa, which may correspond to Lactoferrin (90kDa). The band at 70.3-65.3 kDa is slightly more intense than the previous and it may be correlated to albumin (66kDa). The next band is also present in AMY, which may indicate that amylase is fractionated therefore the band at 56.9-56.7 and 54-53.3 kDa may corresponds to both glycosylated and non-glycosylated forms of α-amylase. The band found at 40.1kDa most probably contains other basic PRPs whilst the band at 25-24.9 kDa corresponds to the acidic PRPs.

The lanes from 6 to 9 present the proteins in the AMY standard. The results show a unique and intense band from 50.9-50.4 kDa indicating that the standard is mainly AMY however given the range of the band it is likely this fraction contains different amylase forms and/or some other proteins with similar molecular weight.

4.2. Zeta potential of proteins

Zeta potential enables the characterization of the electrochemical surface of proteins. When proteins are adsorbed to surfaces several binding types are involved, the

electrostatic, van der Waals, hydrophobic and steric interactions are examples of that. Electrostatic mechanism plays an important role on proteins adsorption and can also be measured by zeta potential. Zeta potential provide information about proteins surface net charge.[5] Zeta potential was performed in order to know the global net charge of proteins present in both saliva and pure α-amylase which represents a great percentage of proteins in human saliva.

Table S-1 – Zeta potential values obtained for the samples.

Samples	Zeta potential, mV
Pure saliva	-10.74
α-amylase	-11.4

The results showed that both proteins samples had negatively charged net, **Table S-1**. The experiments were carried out at pH higher than α-amylase isoelectric point, therefore the negatively charge net was expected. Considering the saliva, it composition is highly complex and the global net charge could be affect by that. Nevertheless, the pure sample saliva also showed to be covered by a negatively charged net.

5. Thickness of AMY and Saliva layer

The most common salivary protein found in saliva[6] is AMY, which represented 40 to 50% of salivary proteins[7].

Regarding this fact, surface packing density estimation for both AMY and Saliva were based on the crystal structure of AMY which presents an ellipsoid shape with dimensions of 7.1, 11.5 and 11.9 nm, respectively.[8] Surface packing densities were calculated based on SPR/LSPR experiments by three approaches. The footprint of each AMY molecule assumed an orthorhombic three dimensional space where the surface area was calculated by $A= \pi \times (C1/2) \times (C2/2)$ where C means the crystal dimensions (C1- 11.5 nm; C2- 11.9 nm and C3- 7.1 nm).

The calculations obtained for SPR indicate that AMY formed a monolayer on the surface (except the footprint A) while saliva seems to form a multilayer. The formation of multilayers for saliva was not a surprise, the presence of different proteins on this complex matrix and several forces between proteins-protein and protein-surface leads to a multilayer formation. Assuming the highest surface density condition the SPR measurements indicate a monolayer thickness of 7 nm.

Whereas for the LSPR calculations, the protein volume was estimated based on the protein thickness obtained by SPR (7 nm). Saliva is a complex matrix which presents several proteins in their composition, such as lactoferrin, human serum albumin, etc therefore it was also assumed a thickness average of 14 nm for salivary proteins. Both SPR and LSPR results are shown in **Table S-2**.

Table S-2–Surface packing density estimation by: SPR and LSPR for both AMY and saliva.

Footprint, nm	Surface Packing Density, %				
	SPR		LSPR		
	AMY	SALIVA	AMY	SALIVA 7 nm	SALIVA 14 nm
A (11.5 × 11.9)	73	266	158	333	535
B (7.1 × 11.9)	45	164	97	206	331
C (7.1 × 11.5)	44	159	94	199	319

6. LSPR Imprinting process

Two different imprinted materials were synthetized in parallel using a single and multiple proteins matrix, resulting in AMY imprinted material (AIM) and pure saliva imprinted material (SIM). The imprinting process and interaction measurements were followed by a Shimadzu UV-VIS-NIR Spectrophotometer UV-360 with wavelength range from 500 to 900 nm.

To create anchor spots for linkage of imprinting polymer on nanodisks gold surface a thiol layer was introduced by incubating over-night 1 mL TPCA 5mM prepared in 10% EtOH with the Au nanodisk substrates. Non-covalent molecular imprinted (MIP) approach was used to prepare the two distinct smart surfaces. For each Au nanodisks substrate, 50 µL AMY 10µM or pure saliva was added for 2h at 4 ºC followed by MQ water rinsing. AMY and saliva remained physically adsorbed on the surface. Two functional monomers, MAA and VTMA 5mM were then added for 30 min each and in this specific order. Both functional monomers and the template (AMY or saliva) interact

through non-covalent binding self-rearranging themselves around the adsorbed protein. Over-night (12h) polymerization was then initiated by adding a 1 mL polymerization mixture containing EDGMA, MA and AP 5 mM to the surface at 39 ºC. After polymerizations ends, the surface was thoroughly rinsed with MQ water. Template removal was carried out by adding 50 µL of Proteinase K 500 µg/mL for 2h at 37 ºC turning the binding sites available for protein rebinding. The molecular imprinting process is shown in **Figure S-3**.

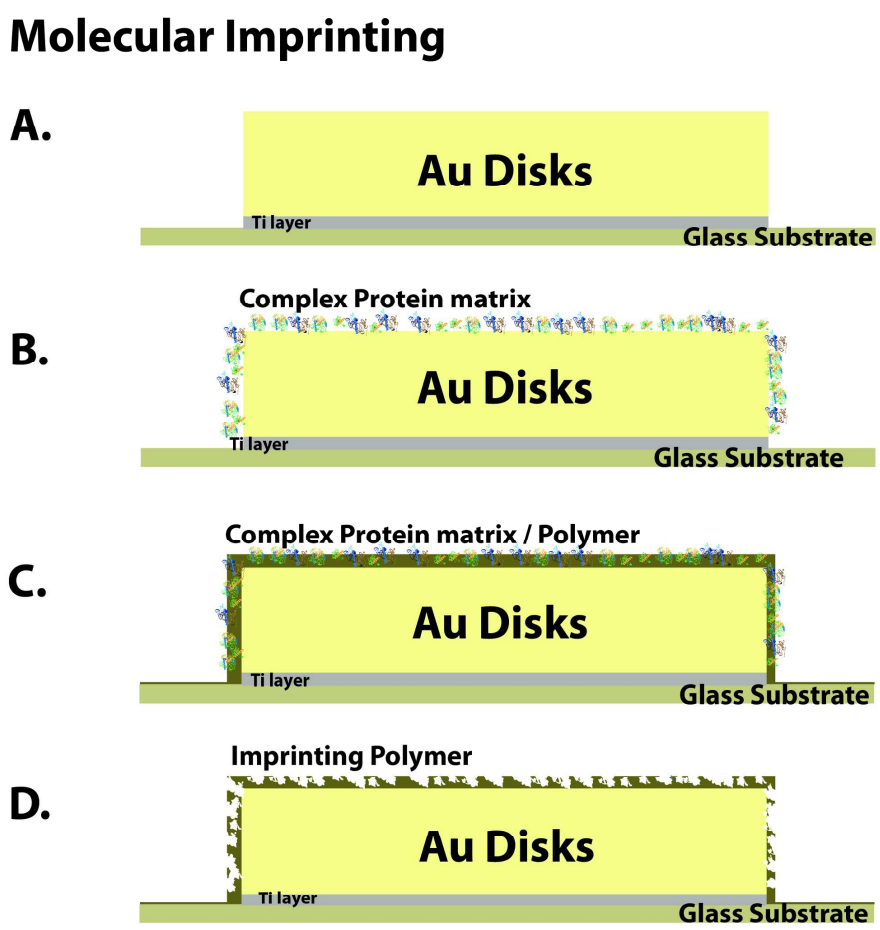

Figure S-3 - Molecular imprinting process: (A) Au disks, (B) Au disks with adsorbed saliva (C) Au disks/Saliva/Polymer, (D) Au disks/Saliva/Imprinting Polymer.

7. Electrochemical assays, independent technique

7.1. Equipment and chemicals

The solutions used for the electrochemical measurements were 2.5 mM $K_3[Fe(CN)_6]_4$ and $K_4[Fe(CN)_6]_3$ prepared in PBS buffer and 250 mM KCl.

The electrochemical measurements were conducted with a potentiostat from Metrohm Autolab, equipped with a FRA module and controlled by Nova software. Cyclic voltammetry, square wave voltammetry and impedance measurements were performed in a three-electrode cell. An Ag/AgCl (3.5 M KCl) electrode and a Pt wire (0.5 mm diameter) were the reference and auxiliary electrodes, respectively.

7.2. Electrodes cleaning procedure

Prior to electrodes (CH Instruments, Austin, Texas, USA; diameter 2 mm) modification a cleaning procedure was applied. First, the electrodes were mechanically polished on a microcloth pad using 1 μm diamond and 0.1 μm alumina slurries (both from Struers, Copenhagen, Denmark), washed with MilliQ water and ultrasonicated in a 1:1 EtOH:H_2O solution for 10 minutes. Then the electrodes were clean electrochemical with 0.5 M KOH followed by 10min Acid Piranha solution (H_2SO_4/H_2O_2). At this point the electrodes were electrochemical polishing in 1 M H_2SO_4 and 1 M H_2SO_4/10mM KCl.

The electrochemical surface area was determined from the gold surface oxide reduction peaks in 0.1 M H_2SO_4. Before any modification, the electrodes were kept in MilliQ water for at least one hour. The obtained electrochemical surface area was 0.094 ± 0.018 cm^2.

7.3. Electrodes edification

The electrochemical measurements were carried out by using a redox pair potassium ferricyanide and potassium ferrocyanide as standard redox probe.

For the edification of the sensor material, gold electrodes were incubated overnight in TPCA 5 mM prepared in aqueous solution 10% EtOH. After rinsing with MilliQ the gold electrodes were incubated with protein (pure saliva or AMY, 10μM) for 2h30 at 4 °C. The electrode was rinsed with MilliQ water, the proteins were physically adsorbed to gold surface. The imprinting process started by adding 10 μL of negative and positive charged monomer for 30 min each; MAA and VTMA both 5mM in MilliQ water. After rinsing the polymerization mixture composed of EGDMA, AP, MA 5mM prepared in Milli-Q was added to the working area of the electrode over night at 40°C. After polymerization, the sensor was thoroughly washed with MilliQ water and incubated in proteinase k for 2h at 37°C. Proteinase k is an enzyme able to break peptide bonds, allowing a successful removal of the protein from the imprinted layer after rinsed.

Electrode modifications were followed by cyclic voltammetry (CV) between - 0.5 and 0.8 V, at a scan rate of 50 mV/s for 3 cycles and electrochemical impedance spectroscopy (EIS) analyzed by electrochemical circle fit from NOVA software which

is based on an equivalent circuit (**Scheme S-1**) based on the Boukamp model. Electrochemical calculations used for system ferricyanide/ferrocyanide a diffusion coefficient value of 0.70 x10^{-5} cm^2/s.

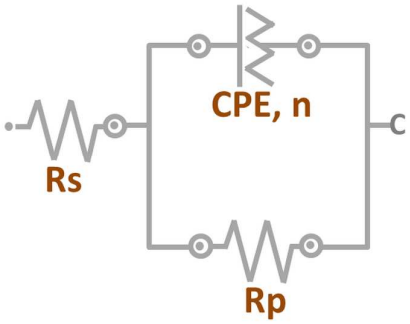

Scheme S-1 –Equivalent circuit used in the electrochemical circle fit. Rs (Ω) simulates the value of the uncompensared resistance, Rp (Ω) charged transfer resistance, CPE or Q constant phase element, n the value of the exponent of the constant phase element.

As it can be seem from **Figure S-4 and Table S-3-S-4,** the reversibility of the ferrycianide/ferrocyanide redox chemistry on Bare Au does change when compared to Au with adsorbed AMY or saliva, the peak separation increases significantly meanwhile the current also decreases. Additionally, AMY and Saliva physically adsorbed on gold electrodes also provides an increase of the charge transfer resistance (R_{ct} or R_p) in the EIS response and decreases the capacitance. Impedance spectra of gold electrodes for both salivary protein and AMY showed the same tendency, the charge transfer resistance increases to 10069±719Ω and 1146±126Ω respectively, whereas for saliva is significantly higher. Proteins adsorption impedes the electron transfer process by blocking the electrode surface promoting the obtained response. Through the CVs is also possible to calculate the surface coverage based on the electrochemical active surface area which showed for saliva 57.6% coverage while for AMY it was 22.1%. When compared to SPR, the electrochemical results provided lower surface coverage which might be due to a different detection method. Both were performed in flat gold surfaces however SPR is very sensitive and the amount of protein on the surface is calculated based on the refractive index, while for electrochemistry proteins are determined based on the diffusion of the probe through the protein layer. Therefore the lower electrochemical surface coverage may indicate that protein layer may help on the probe transfer.

The polymerization process was performed in electrodes with adsorbed proteins (MIP) and in bare Au electrodes (absence of protein -NIP), during this process a growing rigid

polymer network is formed around the adsorbed protein and on the gold surface. To preserve the adsorbed protein conformation during the polymerization, an aqueous environment was the condition selected. The polymer is mainly composed of methyl acrylate monomers promoting hydrogen bonds interactions with the outer surface of target proteins. Additionally, before the beginning of the polymerization the charged monomers were allowed to form a kind of target protein/charged monomers cluster which affects the binding sites formation. Rather than just protein interaction with polymerization materials, the charged monomers also stablish hydrophobic interactions with the polymer, playing an important role on cavities chemistry.

The polymerization provides a decrease on both CVs peak separation and charge transfer resistance for MIP. Alongside, non-imprinted material showed a similar CV peak separation, associated with a slightly decrease of current intensity while ESI spectra showed an increase of charge transfer resistance, proving polymer layer formation. Therefore, the results obtained for the polymerization of the imprinted material indicates that the polymer was form however the resulting combination of proteins and polymer provides the diffusion of the electrochemical probe.

Protein removal from the polymer was performed by proteinase k, the results for non-imprinted material remained nearly the same for both peak separation and charge transfer resistance, consistent with the fact that there was no protein to be extracted. The imprinted materials experienced a reduction in terms of peak separation and the electron transfer ability was regained. On this stage the imprinting materials presented the specific cavities ready to interact with matching proteins during rebind step. Both imprinting and non-imprinted materials were tested for rebinding by incubation with both AMY and saliva. Saliva and AMY imprinted materials showed an increase of both peak separation and charge transfer resistance indicating a protein rebinding. The surface coverage of the imprinted material *versus* the non-imprinted material for saliva was 33.9% and 32.9%, respectively. Whereas for AMY imprinted material it was 5.3% and the non-imprinted had a small rebinding of 0.6% confirming the ability to rebind AMY. According to these results it seems that AMY imprinting material presents lower non-specific binding than saliva imprinted material. The electrochemical control of the imprinted process was used as an additional control of the imprinting process.

Table S-3 – Electrochemical parameters calculated based in Cv and EIS for Saliva

	Material	Bare Au	Au/Saliva	Au/Saliva/ Polymer	Au/Saliva/Polymer/Saliva removal	Au/Saliva/Polymer/Saliva removal/ Saliva Rebinding
ΔE, mV	MIP	72±1	275±10	166±17	96±2	100±14
	NIP	72±4	-	67±1	75±1	116±2
I_{pa}, µA	MIP	22.9±0.6	9.7±0.5	13.6±2.0	24.2±1.4	17.8±0.5
	NIP	23.0±0.5	-	21.8±0.7	23.8±0.6	15.3±1.7
Surface coverage, %	MIP	-	57.6		-	33.9
	NIP	-	-		-	32.9
R_{ct}, kΩ	MIP	0.168±0.004	10.07±0.72	2.53±1.03	0.58±0.13	2.19±2.32
	NIP	0.14±0.01	-	0.16±0.03	0.26±0.03	1.21±0.28
CPE.N	MIP	0.9961±0.0006	0.9968±0.0009	0.9977±0.0005	0.9977±0.0002	0.9978±0.0004
	NIP	0.9963±0.0003	-	0.9961±0.0010	0.9967±0.0012	0.9963±0.0003
C, µF cm^{-2}	MIP	1.76±0.26	0.73±0.16	0.46±0.11	0.50±0.09	0.50±0.07
	NIP	1.66±0.17	-	0.001±0.00001	0.95±0.50	0.87±0.34

Γ –surface coverage calculated from the peak area in CVs using Randles–Sevcik equation.

C-capacitance

Table S-4 – Electrochemical Parameters calculated based on Cv and EIS for AMY

	Material	Bare Au	Au/AMY	Au/AMY/ Polymer	Au/AMY/Polymer/AMY removal	Au/AMY/Polymer/AMY removal/ AMY Rebinding
ΔE, mV	MIP	68±1	136±33	93±11	81±6	100±4
	NIP	70±1	-	69±1	69±1	84±6
I_{pa}, µA	MIP	22.3±0.8	17.9±2.1	18.±1.1	22.0±0.5	21.3±0.4
	NIP	22.2±1.0	-	21.9±0.5	22.6±0.6	22.9±1.4
Γ, %	MIP	-	22.1	-	-	5.3
	NIP	-	-	-	-	0.6
R_{ct}, kΩ	MIP	0.14±0.01	1.43±0.51	0.57±0.15	0.38±0.10	0.82±0.13
	NIP	0.14±0.01	-	0.15±0.02	0.15±0.03	0.46±0.17
CPE.N	MIP	0.9958±0.0003	0.9969±0.0006	0.9979±0.0006	0.9976±0.0004	0.9974±0.0006
	NIP	0.99592±0.00004	-	0.9946±0.0022	0.9967±0.0012	0.9979±0.0004
C, µF cm^{-2}	MIP	1.84±0.11	0.75±0.18	0.30±0.02	0.34±0.03	0.37±0.05
	NIP	1.91±0.04	-	0.17±0.07	0.27±0.05	0.30±0.03

Γ –surface coverage calculated from the peak area in CVs using Randles–Sevcik equation.

C-capacitance

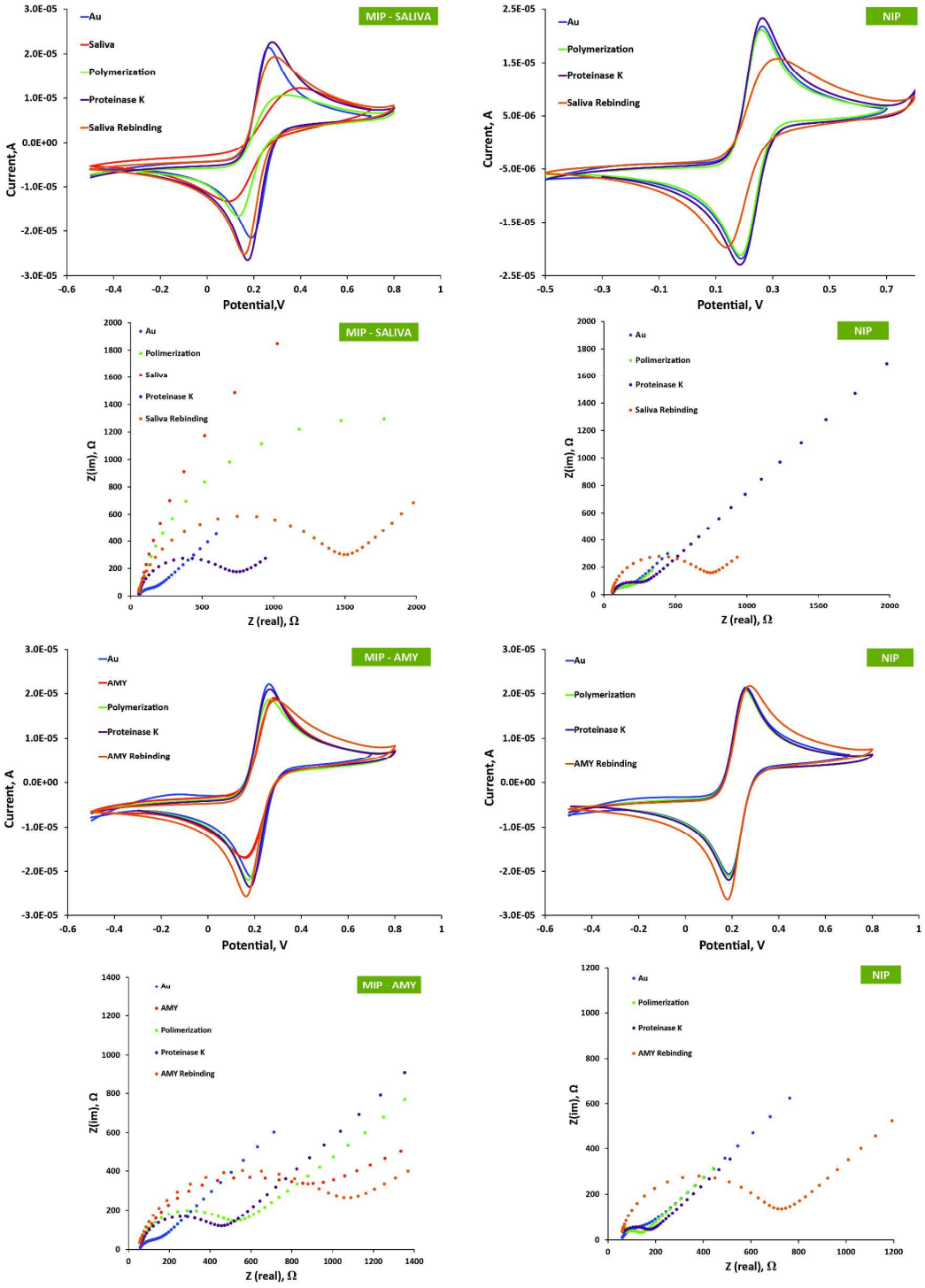

Figure S-4 – CVs and Impedance spectra of MIP and NIP process for both AMY and Saliva.

One of the main goals of the work is the interaction between the proteins captured by the imprinted polymer and study it interaction with a polyphenol compound named PGG. This study was performed by square wave voltammetry.

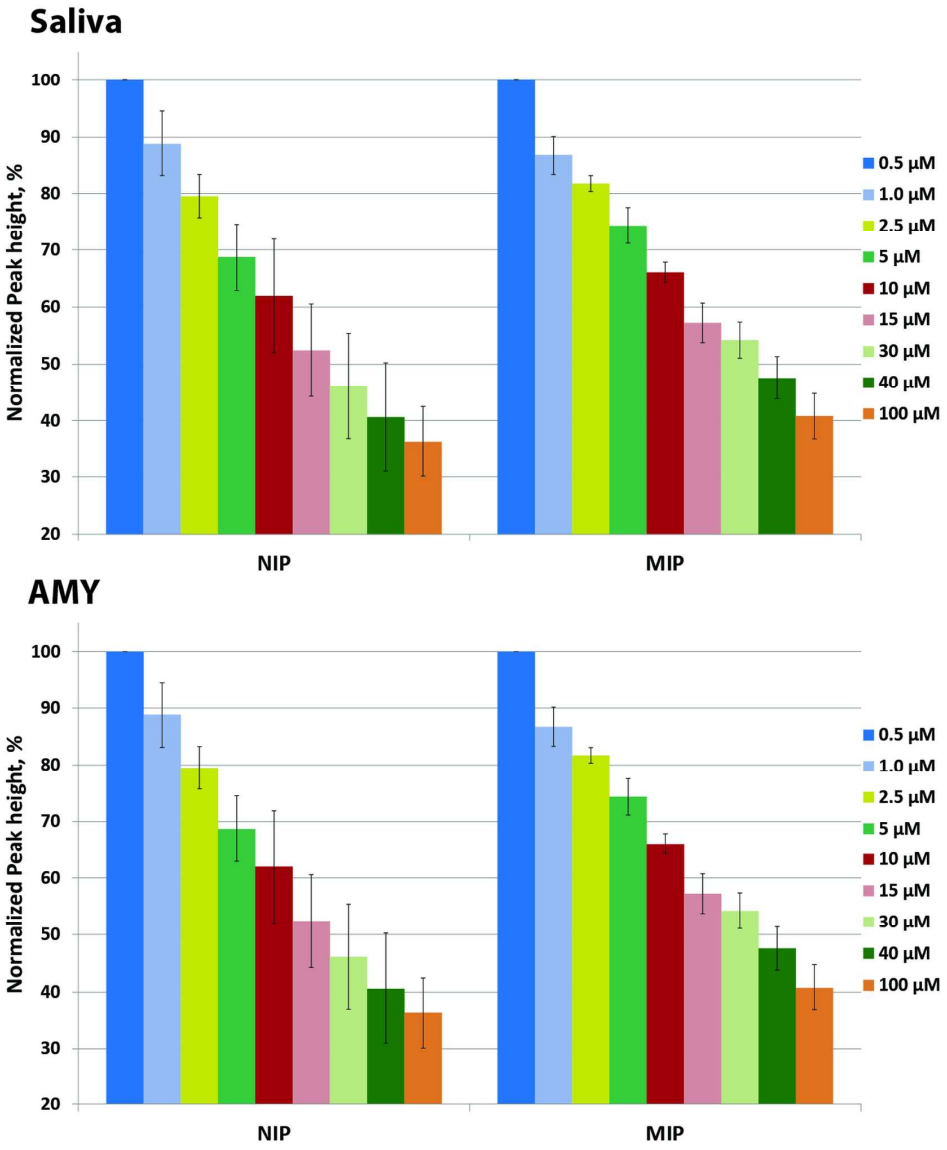

Figure S-5 – Square Wave voltammetry to evaluate the interaction of imprinted and non-imprinted material for both AMY and Saliva

The salivary proteins and AMY imprinted materials were incubated in saliva and pure AMY for rebinding followed by the interaction with PGG standards of different concentration ranging from 0.5 to 100 µM, as can be seen in **Figure S-5**. For both imprinted materials (saliva and AMY) the obtained signal are higher than the non-imprinted response and the standard deviations are smaller. This fact seems to demonstrate that the binding and consequently the interactions are more consistent for imprinting materials. Non-imprinting materials responses indicate a promotion of random non-specific binding of proteins which is translated in significant variation when interacting with polyphenols. Therefore, the imprinting polymer seems to induce bigger interaction detection.

8. Atomic force microscopy

8.1. Au nanodisks

The saliva imprinted material on Au nanodisks substrates was characterized AFM (Bruker Dimension Edge) using silicon probe (RTESP – MPP-11100-10) with spring constant of 20-80 N/m and resonance frequency 200-400 kHz. AFM was performed in tapping mode in air at room temperature, employing a scan size of 1.0 µm and scan rate of 4.0 µm/s. AFM images are present in **Figure S-6** and were analyzed by Nanoscope Analysis.

8.2. Polymer thickness

The thickness of the polymer was investigated by AFM. **Figure S-6** shows a scratched region made on purpose in order to determine the height difference between Ti oxide disks (in the left part of the AFM height image) and 2 nm Ti/20 nm Au/Polymer (in the right of the height image). AFM analysis determined a thickness of ~4 nm on top of Au nanodisks and ~0.5 nm on the glass substrate.

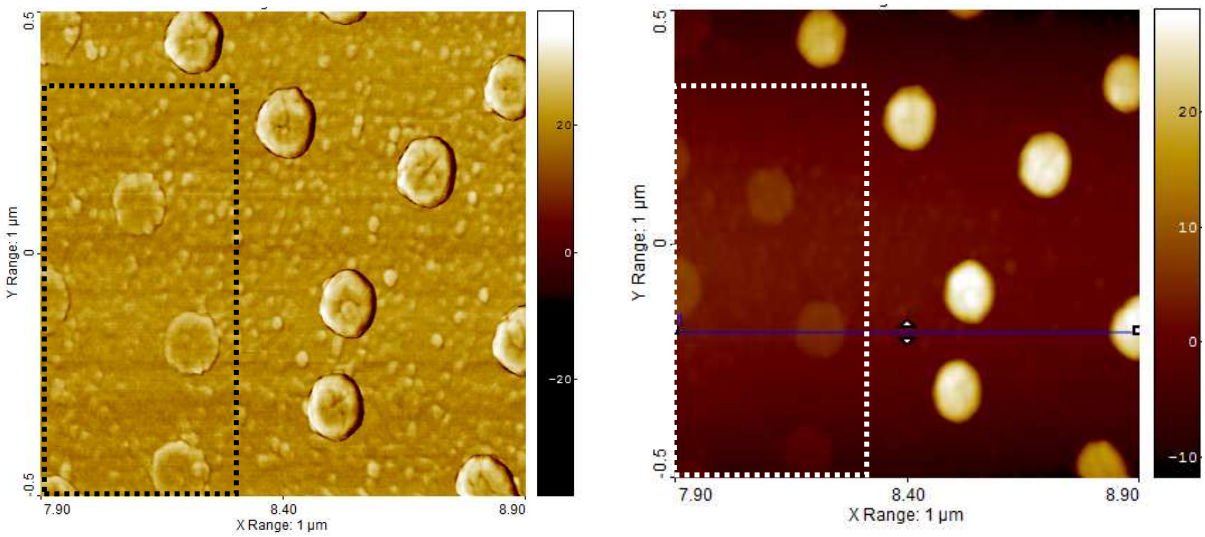

Figure S-6 - AFM images of SIM substrate: phase image (left) and height image (right).

8.3. Peak Force Quantitative Nanomechanical Mapping (PF-QNM): imprinted *vs* non-imprinted polymer

The bare Au nanodisks, amylase imprinted material and non-imprinted material on Au nanodisk samples were characterized by AFM (Bruker, Multimode VIII, Santa Barbara, USA) using PF-QNM mode in liquid under ambient conditions. PF-QNM is a method with which the loading forces can be controlled down to picoNewton levels. This

method is used with optimized operating parameters in order to minimize the damage and artifacts caused by tip.

Imaging was done by depositing twenty microliters of deionized onto sample surface then the tip was immersed in the liquid. Calibration of the equipment was also done in liquid using the same cantilever (Bruker, ScanAsyst-Fluid+cantilever) that was later used for imaging. For this study, cantilevers with nominal spring constant 0.7 N/m were used. The resolution of all PF QNM images is 512 x 512 pixels.

9. LSPR interaction studies

9.1. Polyphenol-Protein interaction

The preparation of smart materials required three main steps, the protein adsorption to the surface, the polymer formation and the protein removal. The smart materials were then exposed to AMY or saliva for protein rebinding followed by the interaction with the selected polyphenols. In order to reuse the smart materials their surface was exposed to proteinase K to remove protein and consequently polyphenol. The summary of the peak shifts obtained for each modification step is presented in **Table S-5**.

Table S-5 – Peak shift promoted by each modification step, for both AIM and SIM materials.

	Peak shift, nm				
Molecular Imprinted Polymer	**Protein**	**Polymer**	**Proteinase K**	**Rebinding**	**Protein Removal**
	red shift	**red shift**	**blue shift**	**red shift**	**blue shift**
AIM	1.94±0.29	0.50±0.01	1.10±0.31	0.99±0.35	0.94±0.40
SIM	4.64±1.04	1.18±0.32	1.81±0.58	1.79±0.28	1.71±0.58

The rebinding step was carried out by adding 100 µL of pure saliva and AMY on SIM or AIM, respectively. All the modification steps were performed in steady state conditions and their evaluation in continuous flow mode using PBS as running buffer while the interaction studies were performed in PBS-E.

Prior to polyphenol interactions and after protein rebinding, the running buffer was replaced by PBS-E, the same buffer used for the preparation of polyphenol solutions, eliminating PBS-E refractive index effect. All polyphenol interacted individually with AMY or saliva, by injecting several standard solutions of increasing concentrations; for

PGG concentrations ranged from 0.1-955μM, for catechin ranged from 160-56500 μM and B3 100-57000 μM

The flow injection system was controlled by a peristaltic pump at the flow rate 50 μL/min, the flowing solutions reach a chamber where the incident light passes through and absorbance is measured. The homemade flow chamber consists of two glass sides (one of them is the Au nanodisks substrate) which work as walls with the flow passing through them.

Prior to polyphenol interaction the LSPR surface with AMY or saliva rebind was placed on the chamber with PBS running buffer followed by the exchange of running buffer for PBS-E and for each spectra was collect. Interaction measurements were performed in PBS-E because this was the buffer used for polyphenol standard solutions. Therefore, it was necessary to know the effect of the buffer refractive index on the LSPR surface with AMY or saliva rebind before the interaction studies.

It is known that polyphenol and protein interactions are quickly established; therefore the settle contact time for interaction was 2.5 minutes followed by an extra 2.5 min buffer wash before spectra collection.

The interaction measurements were then carried out with PGG, Catechin and B3 polyphenol. Increasing concentrations of each polyphenol solutions were injected in the system for 2.5 min followed by running buffer rinsing for extra 2.5 min.

All the spectra were collected after PBS-E running buffer rinsing to assure a stable response. These interactions were studied for PGG concentrations ranging from 0.1 - 955 μM, (+)-catechin ranging from 160-56500 μM and B3 100-57000 μM.

An important note is that substrates should always be placed in the chamber in the same position.

The main characteristics obtained for the different sensors when exposed to the three classes of polyphenol are summarized in **Table S-6**.

Table S-6 – Summary of LSPR sensor characteristics.

Polyphenols	LIRL shift, nm	LSRL shift, nm	Concentratiom, µM
PGG			
SIM – Saliva	0.30±0.17	3.39±0.33	1.6 – 954
NIP-Saliva	0.13±0.11	1.71±0.41	4.1 – 954
AIM - AMY	0.31±0.08	1.54±0.16	4.1 – 954
NIP – AMY	0.07±0.05	1.07±0.78	9.1 – 954
SIM No Protein	0.17±0.09	0.88±0.14	4.1 – 954
Catechin			
SIM – Saliva	0.11±0.004	1.09±0.09	1410 - 56770
NIP-Saliva	0.22±0.26	0.43±0.31	10410 – 56770
AIM - AMY	0.28±0.12	0.52±0.13	1410 – 56770
NIP – AMY	0.12±0.11	0.48±0.26	1410 – 56770
SIM No Protein	0.12±0.15	0.42±0.16	4410 – 56770
B3			
SIM – Saliva	0.22±0.05	1.07±0.01	770 – 56770
NIP-Saliva	0.36±0.24	0.64±0.37	4770 – 56770
AIM - AMY	0.25±0.03	0.84±0.06	770 – 56770
NIP – AMY	0.28±0.21	0.68±0.47	1770 – 56770
SIM No Protein	0.18±0.10	0.35±0.09	770 - 56770

The rebind of AMY on AIM surface within linear region providedd a shift from 0.31±0.08 nm to 1.54±0.16 nm, on NIP 0.07±0.05 nm to 1.07±0.78 nm and AIM surface with no AMY rebind AMY on AIM surface within linear region providedd a shift from 0.31±0.08 nm to 1.54±0.16 nm, on NIP 0.07±0.05 nm to 1.07±0.78 nm and AIM surface with no AMY was 0.17±0.09 nm to 0.88±0.14 nm. The corresponding concentration range for AIM with and without AMY was from 4.1 to 955 µM and 9.1 to

955 μM for NIP. Comparing AIM with AMY and the imprinted material without AMY, the linear responses start at the same concentration, however the shift for the whole range is 2-fold higher when protein is present. For NIP/AMY the shift obtained for the lowest concentration on the linear range is even smaller than for the control with no protein. SIM surface presented the same tendency, where SIM/saliva interacting with PGG provided a shift from 0.30±0.17 nm to 3.39±0.33 nm and for NIP 0.13±0.11 nm to 1.71±0.41 nm. In this case saliva seems to provide bigger shifts if interacting with PGG than with AMY. Again, the imprinted material starts to respond linearly at lower PGG concentration and additionally presents higher peak shifts. In general, the higher peak shifts for the interaction PGG-saliva may be due to other proteins within the saliva which are significantly stronger binders for PGG than AMY. Moreover, different proteins that compose saliva may have variable mobility to rearrange themselves upon binding than AMY molecules.

Similarly to PGG behavior, (+)-catechin interaction with AMY and saliva provided a red shift of plasmon peak with a linear range starting at higher concentrations than the initially injected. Within the linear region, (+)-catechin interacting with AMY on AIM surface provided a shift from 0.28±0.12 nm to 0.52±0.13 nm, for NIP 0.12±0.11 nm to 0.48±0.26 nm and AIM surface with no AMY was 0.12±0.15 nm to 0.42±0.16 nm. Both AMY/AIM and NIP show the linear region in the concentration range from 1410 to 57000 μM and for no AMY/AIM from 4410 to 57000 μM. The results concerning imprinting and no imprinting materials revealed that the lower concentration (on the linear range) provide 2-fold higher shift for the imprinting material. Meaning that the detection of (+)-catechin is more sensitive, although it seems that signal obtained is close to the detection limit. When looking to the imprinted material with no protein, as a control and which represents the worst case scenario, the lowest concentration in the linear range provided a shift close to the NIP. However, much higher concentration (4410μM) was required to achieve the same peak shift. For the SIM surface, when (+)-catechin interacts with saliva, the correspondent shifts ranged from 0.11±0.004 nm to 1.09±0.09 nm and for NIP 0.22±0.26 nm to 0.43±0.31 nm. The NIP material revealed to be only sensitive for much higher concentrations, which resulted in later responses by contrasting the imprinting material. Therefore, the detection of a monomeric unit was feasible for both smart surfaces. The detection of a dimer B3 molecule was also performed. The obtained signal on the linear range for surface AIM with AMY was a shift from 0.25±0.03 nm to 0.84±0.06 nm, for NIP 0.28±0.21 nm to 0.68±0.47 nm and AIM surface with no AMY was 0.18±0.10 nm to 0.35±0.09 nm. For the same shift obtained for both AMY/AIM and AMY/NIP, the non-imprinted material required

higher concentration and the total shift of the linear range is also smaller. When no protein is present, the interaction of B3 with the polymer provides the lowest shift of all surfaces and it has a slightly constant tendency. The results for B3 interacting with saliva/SIM and saliva/NIP demonstrate that the imprinting material has a higher sensitivity since it can detects lower concentrations than the non-imprinted. It also provides a higher total shift in the linear range.

Generally, the interaction detection was more sensitive when imprinted materials were used, **Figure S-7**.

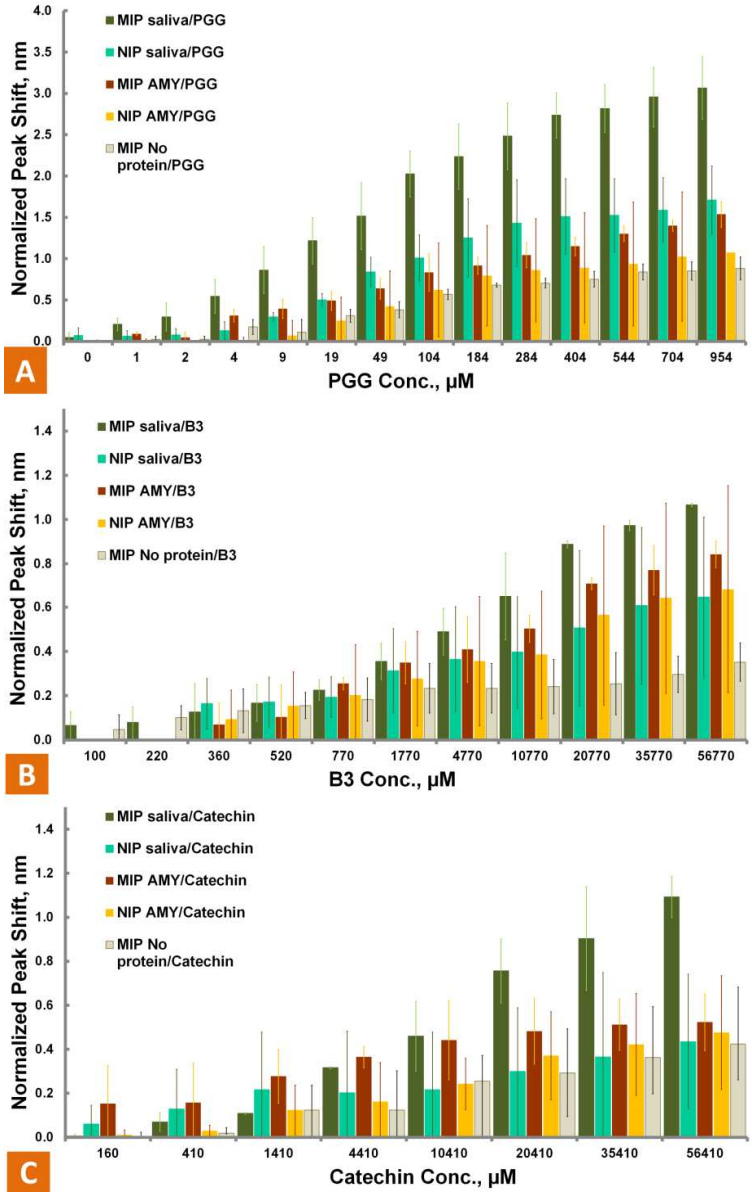

Figure S-7 – Amylase and saliva interaction with (A) PGG, (B) catechin and (C) B3.

On the other hand, the non-imprinted materials seem to provide less accurate shifts presenting higher standard deviations. The LSPR signals for the monomer and dimer (catechin and B3) were significantly lower when compared to PGG, which might be expected from their lower molecular weight.

9.2 LSPR control – low astringency wine matrix effect

In order to study the effect of a complex matrix in the interaction polyphenol-protein, LSPR controls were performed. The complex matrix selected was a low astringency white wine sample spiked with PGG in the range of 1.7–164.2 µM and tested in saliva imprinted materials (SIM) upon saliva rebinding. The wine sample was 1:100 diluted in PBS with 5% ethanol. The calibrations were performed in PBS buffer 5% EtOH and compared with the calibration performed in the presence of the complex matrix also prepared in PBS with 5% ethanol.

The results show that in the presence of a complex matrix some interference is present, as shown in Figure S-8, although the signal was affected in a very systematic way.

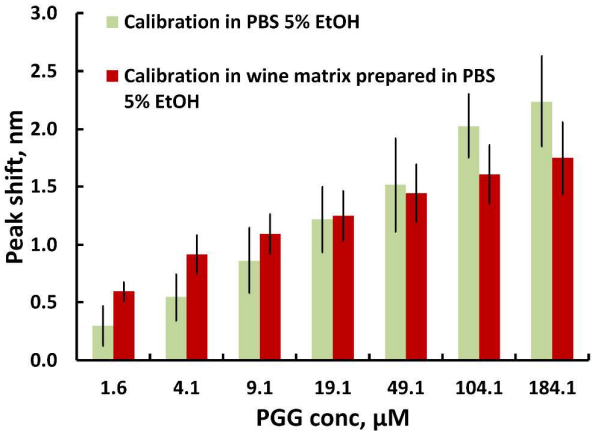

Figure S-8 Effect of a complex wine matrix on the LSPR response for SIM/Saliva and PGG interaction, standard errors of means derived from 3 different samples. “

10.Surface Analysis using LC-MS/MS

The target of the surface analysis by LC-MS/MS was to identify the salivary proteins recognized by the saliva imprinted material. In parallel three controls were performed: i) non imprinted material, ii) saliva imprinted material with no saliva rebinding iii) pure saliva solution. Triplicate samples were incubated with saliva (100 µL) for 2h at 4ºC, rinsed with MQ water followed by trypsin digestion which required the addition of 0.5 mL $(NH_4)HCO_3$ (AMBIC) 50 mM with 3 µg trypsin for 16-24h at 37ºC. The solution used for trypsin digestion was then collected and samples were washed with 1 mL

AMBIC which was combined with the previous solution and stored at -20 ºC. Samples were then lyophilized, dissolved in 100 µL H2O, followed by reduction of Cys residues using 10 mM dithiothreitol (30 min at 23ºC) and alkylation with 30 mM iodoacetamide (1h at 23ºC in the dark). Prior to LC-MS/MS analysis the samples were desalted using POROS 50 R2 material packed in gel loader tips. Desalted samples were lyophilized in a vacuum centrifuge until a final volume of 2-3µL and redissolved with 10 µL of 0.1% formic acid.

LC–MS/MS-analyses were performed using a nano flow HPLC system (Thermo Scientific, EASY-nLC II) connected directly to the mass spectrometer (AB SCIEX TripleTOF 5600 +) equipped with a NanoSpray III source (AB SCIEX) and operated under Analyst TF 1.6.0 control. The samples were injected, trapped and desalted isocratically on a fritted fused silica capillary pre-column (100 µm i.d. × 2 cm) packed with ReproSil-Pur C18-AQ 3 µm resin (Dr. Maisch GmbH, Ammerbuch-Entringen, Germany), separated on a fused silica capillary column (75 µm i.d x 15 cm) and electrosprayed into the mass spectrometer. The capillary column was pulled into a tip on a P-2000 laser based micropipette puller (Sutter Instrument Co.) and packed with ReproSil-Pur C18-AQ 3 µm resin (Dr. Maisch GmbH, Ammerbuch-Entringen, Germany). The elution was performed at a flow rate of 250 nL/min using a 50 min gradient from 5-35% phase B (0.1% formic acid in 90% acetonitrile). Information-dependent acquisition (IDA) experiment using up to 50 MS/MS spectra in each 2.3 s cycle was set up. An exclusion window of 10 s was used. The MS files were searched against the Swiss-Prot (version 2015_01) *Homo sapiens* database (20,200 sequences) using Mascot Daemon software (version 2.5.0). The significance threshold (p) was set to 0.01 with an expect cutoff of 0.005. Trypsin was set as the digestion enzyme and one missed cleavage was allowed. Carbamidomethyl was selected as a fixed modification for Cys residues and carbamylation of Lys residues, oxidation of Met residues, and deamidation of Asn and Gln were set as variable modifications. Mass tolerances of 10 ppm and 0.2 Da were set for the precursor and product ions, respectively. Mascot data were parsed using MS data miner (version 1.3.0)[9].

The proteins identified both in pure saliva and in the saliva imprinted material after saliva rebinding are shown in **Table S-7**. The saliva imprinted material with saliva rebinding detected 36 proteins out of 101 proteins found in pure saliva. The code correspondents to each protein is the catalog reference from the UniProt (Universal Protein Resource).

Table S-7 – Proteins identification by MS/MS.

Proteins identification			
Protein code	**Saliva**	**Protein code**	**Substrate MIP Saliva/Saliva rebinding**
Q7Z5M8	Abhydrolase domain-containing protein 12B	P62736	Actin, aortic smooth muscle
P62736	Actin, aortic smooth muscle	P01009	Alpha-1-antitrypsin
P01009	Alpha-1-antitrypsin	P04745	Alpha-amylase 1
P01023	Alpha-2-macroglobulin	P03973	Antileukoproteinase
P04745	Alpha-amylase 1	P02647	Apolipoprotein A-I
P03973	Antileukoproteinase	Q96DR5	BPI fold-containing family A member 2
P02647	Apolipoprotein A-I	Q8TDL5	BPI fold-containing family B member 1
Q68CP9	AT-rich interactive domain-containing protein 2	P23280	Carbonic anhydrase 6
P61769	Beta-2-microglobulin	P22528	Cornifin-B
Q96DR5	BPI fold-containing family A member 2	P28325	Cystatin-D
Q8TDL5	BPI fold-containing family B member 1	P01036	Cystatin-S
Q8N4F0	BPI fold-containing family B member 2	P54108	Cysteine-rich secretory protein 3
P62158	Calmodulin	Q9UGM3	Deleted in malignant brain tumors 1 protein
Q9NZT1	Calmodulin-like protein 5	P06396	Gelsolin
P23280	Carbonic anhydrase 6	P69905	Hemoglobin subunit alpha
Q02388	Collagen alpha-1(VII) chain	P01876	Ig alpha-1 chain C region
P01024	Complement C3	P01877	Ig alpha-2 chain C region
P35321	Cornifin-A	P01857	Ig gamma-1 chain C region
P22528	Cornifin-B	P01859	Ig gamma-2 chain C region
P04080	Cystatin-B	P01860	Ig gamma-3 chain C region
P01034	Cystatin-C	P0CG05	Ig lambda-2 chain C regions
P28325	Cystatin-D	P01871	Ig mu chain C region
P01036	Cystatin-S	P01591	Immunoglobulin J chain
P09228	Cystatin-SA	P35527	Keratin, type I cytoskeletal 9

P01037	Cystatin-SN	P04264	Keratin, type II cytoskeletal 1
P54108	Cysteine-rich secretory protein 3	P22079	Lactoperoxidase
Q9UGM3	Deleted in malignant brain tumors 1 protein	P61626	Lysozyme C
Q9BPU6	Dihydropyrimidinase-related protein 5	Q8TAX7	Mucin-7
Q9BRZ2	E3 ubiquitin-protein ligase TRIM56	P12273	Prolactin-inducible protein
Q6ZMW3	Echinoderm microtubule-associated protein-like 6	P31949	Protein S100-A11
Q6JVE6	Epididymal-specific lipocalin-10	P06703	Protein S100-A6
P04075	Fructose-bisphosphate aldolase A	P05109	Protein S100-A8
Q08380	Galectin-3-binding protein	P06702	Protein S100-A9
P06396	Gelsolin	P02768	Serum albumin
P69905	Hemoglobin subunit alpha	Q9UBC9	Small proline-rich protein 3
P02042	Hemoglobin subunit delta	Q9P0W8	Spermatogenesis-associated protein 7
P02008	Hemoglobin subunit zeta		
P02790	Hemopexin		
P01876	Ig alpha-1 chain C region		
P01877	Ig alpha-2 chain C region		
P01857	Ig gamma-1 chain C region		
P01859	Ig gamma-2 chain C region		
P01860	Ig gamma-3 chain C region		
P01861	Ig gamma-4 chain C region		
P01766	Ig heavy chain V-III region BRO		
P01768	Ig heavy chain V-III region CAM		
P01834	Ig kappa chain C region		
P01597	Ig kappa chain V-I region DEE		
P01605	Ig kappa chain V-I region Lay		
P01612	Ig kappa chain V-I region Mev		
P01616	Ig kappa chain V-II region MIL		

P06310	Ig kappa chain V-II region RPMI 6410
P01621	Ig kappa chain V-III region NG9
P01620	Ig kappa chain V-III region SIE
P04433	Ig kappa chain V-III region VG
P04434	Ig kappa chain V-III region VH
P04211	Ig lambda chain V region 4A
P06888	Ig lambda chain V-I region EPS
P01700	Ig lambda chain V-I region HA
P80748	Ig lambda chain V-III region LOI
P01714	Ig lambda chain V-III region SH
P0CG05	Ig lambda-2 chain C regions
P01871	Ig mu chain C region
Q9Y6R7	IgGFc-binding protein
P01591	Immunoglobulin J chain
B9A064	Immunoglobulin lambda-like polypeptide 5
P06870	Kallikrein-1
P13645	Keratin, type I cytoskeletal 10
P35527	Keratin, type I cytoskeletal 9
P04264	Keratin, type II cytoskeletal 1
Q7Z794	Keratin, type II cytoskeletal 1b
P35908	Keratin, type II cytoskeletal 2 epidermal
A4D1S0	Killer cell lectin-like receptor subfamily G member 2
P22079	Lactoperoxidase
P31025	Lipocalin-1
Q99698	Lysosomal-trafficking regulator
P61626	Lysozyme C
Q9HC84	Mucin-5B

Q8TAX7	Mucin-7
P24158	Myeloblastin
P59665	Neutrophil defensin 1
P08246	Neutrophil elastase
P80188	Neutrophil gelatinase-associated lipocalin
Q9H0G5	Nuclear speckle splicing regulatory protein 1
P80303	Nucleobindin-2
P13796	Plastin-2
P01833	Polymeric immunoglobulin receptor
Q6PIU1	Potassium voltage-gated channel subfamily V member 1
P12273	Prolactin-inducible protein
P31949	Protein S100-A11
P06703	Protein S100-A6
P05109	Protein S100-A8
P06702	Protein S100-A9
Q8TF72	Protein Shroom3
Q8TAB3	Protocadherin-19
Q14602	Putative DNA-binding protein inhibitor ID-2B
Q8IWN7	Retinitis pigmentosa 1-like 1 protein
P52566	Rho GDP-dissociation inhibitor 2
Q92974	Rho guanine nucleotide exchange factor 2
P38159	RNA-binding motif protein, X chromosome
Q13523	Serine/threonine-protein kinase SMG1
P02787	Serotransferrin
P02768	Serum albumin
Q9UBC9	Small proline-rich protein 3
Q9P0W8	Spermatogenesis-associated protein 7

Q9H7N4	Splicing factor, arginine/serine-rich 19
Q5VSL9	Striatin-interacting protein 1
P10599	Thioredoxin
P37837	Transaldolase
P20061	Transcobalamin-1
Q70CQ1	Trypsin-1
P62979	Ubiquitin carboxyl-terminal hydrolase 49
Q68DL7	Ubiquitin-40S ribosomal protein S27a
Q6P5S2	Uncharacterized protein C18orf63
P02774	UPF0762 protein C6orf58
Q14508	Vitamin D-binding protein
Q8N3Z6	WAP four-disulfide core domain protein 2
P25311	Zinc finger CCHC domain-containing protein 7
Q96DA0	Zinc-alpha-2-glycoprotein
Q7Z5M8	Zymogen granule protein 16 homolog B

References

1. Chen, Y. M.; Hagerman, A. E. Characterization of soluble non-covalent complexes between bovine serum albumin and beta-1,2,3,4,6-penta-O-galloyl-D-glucopyranose by MALDI-TOF MS. *J. Agric. Food Chem.* **2004,** 52, (12), 4008-4011.

2. Fernandes, A.; Fernandes, I.; Cruz, L.; Mateus, N.; Cabral, M.; de Freitas, V. Antioxidant and Biological Properties of Bioactive Phenolic Compounds from Quercus suber L. *J. Agric. Food Chem.* **2009,** 57, (23), 11154-11160.

3. Bras, N. F.; Goncalves, R.; Fernandes, P. A.; Mateus, N.; Ramos, M. J.; de Freitas, V. Understanding the Binding of Procyanidins to Pancreatic Elastase by Experimental and Computational Methods. *Biochemistry.* **2010,** 49, (25), 5097-5108.

4. Hanarp, P.; Sutherland, D. S.; Gold, J.; Kasemo, B. Control of nanoparticle film structure for colloidal lithography. *Colloids and Surfaces a-Physicochemical and Engineering Aspects.* **2003,** 214, (1-3), 23-36.

5. Salgin, S.; Salgin, U.; Bahadir, S. Zeta Potentials and Isoelectric Points of Biomolecules: The Effects of Ion Types and Ionic Strengths. *International Journal of Electrochemical Science.* **2012,** 7, (12), 12404-12414.

6. Vitorino, R.; Lobo, M. J. C.; Ferrer-Correira, A. J.; Dubin, J. R.; Tomer, K. B.; Domingues, P. M.; Amado, F. M. L. Identification of human whole saliva protein components using proteomics. *Proteomics.* **2004,** 4, (4), 1109-1115.

7. Noble, R. E. Salivary alpha-amylase and lysozyme levels: a non-invasive technique for measuring parotid vs submandibular/sublingual gland activity. *Journal of oral science.* **2000,** 42, (2), 83-86.

8. Machius, M.; Vertesy, L.; Huber, R.; Wiegand, G. Carbohydrate and protein-based inhibitors of porcine pancreatic alpha-amylase: Structure analysis and comparison of their binding characteristics. *J. Mol. Biol.* **1996,** 260, (3), 409-421.

9. Dyrlund, T. F.; Poulsen, E. T.; Scavenius, C.; Sanggaard, K. W.; Enghild, J. J. MS Data Miner: A web-based software tool to analyze, compare, and share mass spectrometry protein identifications. *Proteomics.* **2012,** 12, (18), 2792-2796.